How well-mixed is well mixed? Hydrodynamic-biokinetic model integration in an aerated tank of a full-scale water resource recovery facility

Usman Rehman, Wim Audenaert, Youri Amerlinck, Thomas Maere, Marina Arnaldos and Ingmar Nopens

ABSTRACT

Current water resource recovery facility (WRRF) models only consider local concentration variations caused by inadequate mixing to a very limited extent, which often leads to a need for (rigorous) calibration. The main objective of this study is to visualize local impacts of mixing by developing an integrated hydrodynamic-biokinetic model for an aeration compartment of a full-scale WRRF. Such a model is able to predict local variations in concentrations and thus allows judging their importance at a process level. In order to achieve this, full-scale hydrodynamics have been simulated using computational fluid dynamics (CFD) through a detailed description of the gas and liquid phases and validated experimentally. In a second step, full ASM1 biokinetic model was integrated with the CFD model to account for the impact of mixing at the process level. The integrated model was subsequently used to evaluate effects of changing influent and aeration flows on process performance. Regions of poor mixing resulting in non-uniform substrate distributions were observed even in areas commonly assumed to be well-mixed. The concept of concentration distribution plots was introduced to quantify and clearly present spatial variations in local process concentrations. Moreover, the results of the CFD-biokinetic model were concisely compared with a conventional tanks-in-series (TIS) approach. It was found that TIS model needs calibration and a single parameter set does not suffice to describe the system under both dry and wet weather conditions. Finally, it was concluded that local mixing conditions have significant consequences in terms of optimal sensor location, control system design and process evaluation.

Key words | activated sludge modelling, computational fluid dynamics, model integration, wastewater treatment, water resource recovery

Usman Rehman (corresponding author)
Wim Audenaert
Youri Amerlinck
Marina Arnaldos
Ingmar Nopens
BIOMATH, Department of Mathematical Modelling, Statistics and Bio-Informatics,
Ghent University,
Coupure Links 653,
Ghent 9000,
Belgium
E-mail: *usman.rehman@ugent.be*

Thomas Maere
modelEAU, Département de génie civil et de génie des eaux,
Université Laval,
1065 Avenue de la Médecine,
Québec, QC, G1 V 0A6
Canada

Marina Arnaldos
Acciona Agua S.A., R&D Department,
Av. De les Garrigues 22,
El Prat del Llobregat,
Barcelona 08820,
Spain

INTRODUCTION

Water resource recovery facility (WRRF) modelling, and activated sludge modelling in particular, has been increasingly applied in the last couple of decades. Activated sludge models (ASM) have proven to be a useful tool for process evaluation, design and optimization (Fenu *et al.* 2010; Hauduc *et al.* 2013). However, mostly in current modelling efforts, a simplified approach tanks-in-series (TIS) modelling is employed. In TIS modelling, detailed spatial variations in substrate and electron acceptor concentrations in bioreactors (stemming from design characteristics and operational conditions) are typically not taken into account, even though it is plausible that they could have a significant impact on model predictions. Therefore, these models could be unsuitable to evaluate the detailed impact of certain design parameters (such as tank geometry, number and type of propellers, aerator system design, on the performance of the biological process), as well as different operational strategies, if this belongs to the goal of the modelling study. Computational fluid dynamics (CFD) is a modelling method that can be applied to visualise the extent of local hydraulic conditions as a function of design parameters and operational strategies. Currently, this

doi: 10.2166/wst.2017.330

modelling framework is mainly used for basic hydraulic design and troubleshooting. However, when integrated with biokinetic models, it becomes a powerful tool to gain detailed insight into the impact of local mixing conditions in the reactor on overall process performance and thus to be used for developing next generation of flow sheet models (Laurent *et al.* 2014).

The potential of CFD to improve biokinetic model predictions has already been shown in various studies. It was demonstrated that improved systemic model structures can be generated by incorporating knowledge from CFD (Alex *et al.* 2002, 1999). The application potential of combined CFD and ASM models in both pilot- and full-scale systems was evaluated by Glover *et al.* (2006), concluding that it can provide a more accurate description of system oxygenation capacity. Le Moullec *et al.* (2011) used CFD results to create a compartmental model for a pilot plant reactor showing better results than the conventional systemic approach (i.e. TIS) and requiring less computational power than CFD. The potential impact of sensor location in a mixing-limited system on controller performance was demonstrated through the use of a CFD model by Rehman *et al.* (2015), while detailed aeration modelling has been performed in terms of oxygen mass transfer at full scale by Fayolle *et al.* (2007) to show the impact of different operational conditions on mixing. However, it is important to note that these previous efforts did not entail complete ASM-CFD integration at full scale along with detailed modelling of the aeration system, but were limited to either laboratory scale or to only aeration modelling without complete ASM integration. An integrated CFD-ASM model will quantify the impact of local concentration gradients on the overall performance and such that more accurate and objective oriented compartmental models can be developed.

The ASM models are based on a Monod formulation (Monod 1942), which has been extensively used for modeling biological processes in wastewater treatment. In Monod's formulation, microbial growth (and thus substrate consumption) largely depends on local substrate and electron acceptor concentrations (dissolved oxygen (DO), ammonium, etc.) and these dependencies are described by half saturation indices or K-values (Henze *et al.* 1987; Arnaldos *et al.* 2015). The K-values are usually experimentally measured or calibrated for different substrates in the context of different biological processes. However, it is observed that the K-values show high degree of variability and are not consistent between different publications (Arnaldos *et al.* 2015). These differences are normally explained by diffusional or biological limitations in different systems. However, Arnaldos *et al.* (2015) pointed out that advective limitations (arising due to incomplete mixing), that might be present in a system, are not explicitly taken into account while measuring or calibrating K-values. While the biokinetic models have uncertainties regarding the K-values, the conventional TIS modelling approach also has its limitation in terms of its inability to take spatial heterogeneities into account. Therefore, by using TIS approach, there is always a tendency of over calibration of kinetic parameters by correcting errors which are induced by hydrodynamic limitations. Hence, there is a need of detailed hydrodynamic modelling to be included to correctly calibrate and partly avoid the unnecessary and erroneous calibration efforts.

The main objectives of this paper are therefore (1) to provide an evidence that incomplete mixing leads to local heterogeneities in species concentrations and (2) to demonstrate the applicability and added value of integrated CFD-ASM models for process analysis and evaluation for full-scale systems (i.e. knowledge buildup). In order to achieve this principal objective, first, the hydrodynamics of the aeration compartment of a full-scale plant were simulated using CFD and validated experimentally. In a second step, the CFD model was integrated with an ASM to describe the impact of local mixing conditions on biological process performance. The integrated model was then used to analyze consequences at the process level of changing influent and aeration flows. Moreover, we introduced the concept of concentration distribution plots (CDPs) in order to quantify the heterogeneity of species concentrations. In addition, a simple TIS model was also included in the paper to evaluate the consequences of using conventional methods. Henceforth, the impact of K-values on concentrations and process rates was briefly discussed. The usefulness of employing this integrated CFD-ASM approach in terms of determining sensor location, control system design and process evaluation was briefly addressed as well.

MATERIALS AND METHODS

The full-scale plant modelled in this study was the Eindhoven WRRF (The Netherlands). This plant treats wastewater of 750,000 population equivalents (PE) with a design load of 136 g chemical oxygen demand (COD) day^{-1} PE^{-1}. Incoming wastewater is treated in three parallel lines, each containing a primary settler, a biological tank and four secondary settlers. The plant is a modified UCT (University of Cape Town) configuration (biological COD, N and P removal). The circular inner ring (anaerobic) is intended

to be a plug flow reactor, consisting of four compartments in series, with no aeration and minimal recycled nitrate. The carrousel-type middle ring is anoxic and flows over into the outer ring, which has membrane plate aerators in certain locations and is consequently a facultative aerobic/anoxic ring. Two zones of aerators can be distinguished: the 'summer package', which is always active and its airflow is controlled by a NH_4-DO cascade controller accounting for the load, and 'winter package', which can be switched on during winter time or rain events to provide additional nitrification capacity for increased loads. Finally, three recycles are active: one to recycle sludge from the anoxic middle to the anaerobic inner ring, a second one to recycle nitrate from the outer ring to the anoxic middle ring, and a third one to recycle settled secondary sludge to the anoxic middle ring. In this study, the outer ring of one of the three biological reactors of the Eindhoven WRRF has been modelled (Figure 1(a)). The outer ring is 17,000 m^3 in volume and is 7 m deep.

CFD modelling

First, geometry of the aeration tank was created in a commercial tool AutoCAD® (Autodesk) taking into account all the details which can influence reactor hydrodynamics (Figure 1(b)). One of the most significant improvements to the model as compared to previously reported studies was detailed modelling of the aerators. 196 plate aerators (diffusers) are installed at the bottom of the reactor. Practically, it is not feasible to model individual pores on plates. Therefore, in this study, the aeration plates were modelled individually such that each plate represented total area of the pores on a plate keeping geometric symmetry with real plates. Next, meshing using a commercial mesh generator tool (ICEM CFD, ANSYS) was performed. The mesh was kept as structured as possible with 90% of the cells being hexahedrons. Different meshes (0.7, 1.5 and 2.5 million cells) were generated to check for grid independence. The 1.5 and 2.5 million cells mesh provided best match with velocity measurements but the 1.5 million cells mesh was used for all the simulations due to its reduced computational demand. For a steady state solution, the 1.5 million cells mesh took about 3–4 h to converge as compared to 5–7 h for the 2.5 million cells mesh. Subsequently, CFD simulations for the hydrodynamics part were performed in FLUENT (v14.5) (ANSYS).

The mixture model (Eulerian two-fluid model) was used for modeling multi-phase (gas/liquid) flow because the calculation of movement of individual bubbles is difficult in a full-scale plant, whereas this model depicts average movement of a secondary phase (bubbles) (Versteeg & Malalasekera 2007). The relative velocity of the phases was modeled by solving an extra equation for the slip velocity. Turbulence was modeled with Realizable k-ϵ model and the drift velocity model was incorporated to model the dispersion of bubbles by turbulent flow. The drift velocity is important for better prediction of the gas hold-up (Talvy *et al.* 2007). Moreover, standard wall functions were used for the flow near the walls (Manninen

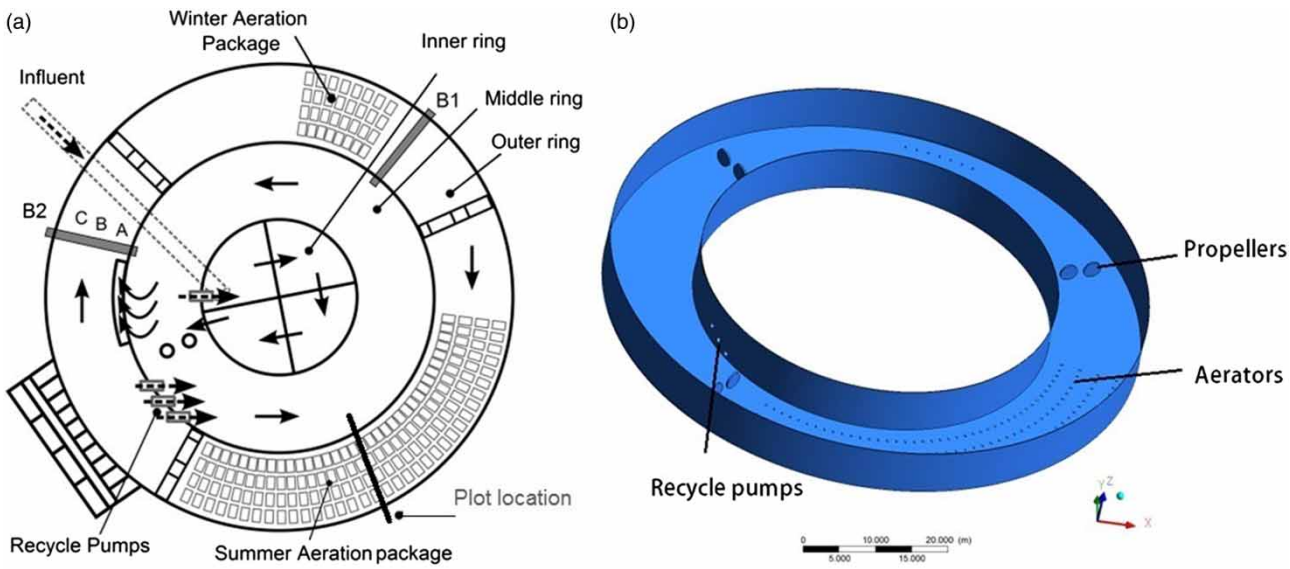

Figure 1 | (a) Reactor configuration and (b) computer aided design of the reactor.

et al. 1996). Development of these models (Ishii & Hibiki 2011) is considered standard so the model details are not described here. However, governing equations of momentum and drift and slip velocity are provided in the Appendix (mixture model) (available with the online version of this paper). Initially, standard water and air properties (density, viscosity, etc.) at 20 °C were used but later during the validation procedure a more realistic sludge density based on suspended solids concentration (De Clercq 2003) was implemented. The effect of gravity was also incorporated in the solution of the Navier-Stokes equations. The free top surface of the reactor was modelled using degassing boundary condition for the gas phase and the symmetry boundary condition for the liquid phase. The mixing propellers were modelled by inducing a constant source of momentum at their corresponding location in the reactor. The momentum source was calculated based on the propellers' energy consumption and their geometrical design (i.e. blade size and type) (Atif et al. 2010).

Experimental setup

In order to validate the hydrodynamics, velocity measurements with the help of an Acoustic Doppler Current Profiler (ADCP) (Teledyne RD) were performed at two bridges (B1 & B2) (Figure 1(a)). Measurements at a third bridge were too disturbed by aeration and thus could not be used for validation purposes. Time-averaged axial and tangential velocity components at different depths were measured at three radial locations at each bridge (A, B & C). At each location for every measurement, 15 min of data were collected and each measurement was repeated three times to reduce the errors induced by the dynamic inflow.

CFD-biokinetic integration

In a next step, given the objective to predict aerobic carbon and nitrogen removal, the model was extended with a biokinetic model, i.e. the well-established Activated Sludge Model No. 1 (ASM1) (Henze et al. 2000, 1987). This integration was performed by adding 13 user defined scalars (UDS) representing each of the 13 components in the ASM1 model (ANSYS Inc. 2011). FLUENT solves 13 transport equations for these UDS. Each transport equation for a scalar $\varnothing$ can generally be written as in Equation (1).

$$\frac{\partial \alpha_l \rho_l \varnothing_l^k}{\partial t} + \nabla.\left(\alpha_l \rho_l \vec{u}_l \varnothing_l^k - \alpha_l \Gamma_l^k \nabla \varnothing_l^k\right) = S_l^k \quad k = 1, \ldots, N \tag{1}$$

Here, α_l, ρ_l and $\vec{u}_l$ are the volume fraction, density and relative velocity of the liquid phase, respectively. $\boldsymbol{\Gamma}$ and $\boldsymbol{S}$ are the diffusion coefficient and the source term for scalar $\varnothing$. $\boldsymbol{k}$ is the corresponding scalar and N is the total number of scalars (in this case 13). The first term in the equation is the unsteady term, which in this case is zero as only steady-state simulations were performed. The source terms were introduced by means of user defined functions based on mass balance equations for each of the ASM1 components. The recommended standard values for all the stoichiometric and kinetic parameters were used (Henze et al. 1987). The results and discussion in this paper are limited to only dissolved oxygen and ammonium due to a lack of space and for improved clarity in conveying the message and reasoning.

In addition to all the standard processes of ASM1, an extra term for the oxygen mass balance was included describing mass transfer from gas to the liquid phase. The local oxygen mass transfer was modelled using Equation (2).

$$J = K_L a\ (Cs - Co) \tag{2}$$

Here, J is the local mass flux, K_L the mass transfer coefficient and a the interfacial area. K_L is calculated using the classical penetration theory (Higbie 1935) based on the diffusion coefficient of oxygen in water at 20 °C, and the interfacial area a is based on bubble size and local volume fractions (Fayolle et al. 2007). The coalescence and breakage phenomenon of the bubbles was not considered and thus a constant bubble size was assumed; an assumption that will be relaxed in the future. The membrane aerators are designed to provide a bubble size of about 3 mm.

Given the importance of density in reactive flows (Samstag et al. 2012; Samstag & Wicklein 2014), bulk density was defined as a function of local suspended solids concentration (De Clercq 2003) (Equation (3)).

$$\rho_b = \frac{\rho_l}{1 - \Phi_s\left(1 - \frac{\rho_l}{\rho_s}\right)} \tag{3}$$

where Φ_s is the local mass fraction of suspended solids, ρ_b the bulk density and ρ_l & ρ_s the liquid and solids density, respectively. Solids density has been reported to range between 1,250 and 1,450 kg/m^3 (Lyn et al. 1992; Stamou et al. 2000). In this study, 1,450 kg/m^3 was used. On the other hand, because turbulent viscosity was dominant due to high turbulence in the tank; the viscosity of water at 20 °C was used instead of viscosity of sludge (Wilcox 1998).

Simulations were performed sequentially such that the simulations for biokinetic equations were performed on top of the 'frozen' converged steady state hydrodynamic solution (at selected liquid and gas flow rates) to reduce the convergence time. Computational requirements to achieve convergence increased significantly from a 3–4 h to 8–10 h after including all the biokinetic equations for the steady-state solution (using eight parallel processors). It is important to mention that convergence time for the next simulation was significantly reduced to 4–6 h when the solution was initialized from a previous converged steady state solution. The influent flowrate and composition is collected from the available plant historical data to use as inlet boundary condition and is provided in the form of ASM1 components in Appendix 1 (available with the online version of this paper). As the inlet data to outer ring is not directly measured so it was borrowed from the Eindhoven WWTP model developed by Amerlinck (2015).

Simulation setups

Several simulations using the CFD-ASM model were carried out to investigate impact of different realistic combinations of liquid and air flow rates on local distribution of substrates and thus process performance. The combination of two influent liquid flow rates and two air flow rates have been simulated to produce a total of four scenarios. The low inflow rate was selected to be Eindhoven's WRRF average dry weather flow (1,876 m^3/h referred to as scenario 'L'), while the high inflow rate was double that (scenario '2 L'). Similarly, the low gas flow rate was also chosen to be the process base case (2,000 Nm^3/h referred to 'G') and the high gas flow rate was three times that ('3G') representing the aeration rate at high peak load conditions. These scenarios were selected based on investigation of long-term flow dynamics in the plant.

As traditional half-saturation indices in ASM models lump several processes (Arnaldos *et al.* 2015), and given the fact that the advection portion of this is explicitly modelled in CFD, it can be expected that K-values used in a combined ASM-CFD model have to be lower. To demonstrate this impact, the half saturation index of dissolved oxygen for autotrophic growth ($K_{O,A}$) was reduced by 15% to study its impact on local concentrations and process rates. The expression for the autotrophic growth rate (Henze *et al.* 1987) is given by Equation (4):

$$Autotrophic\ growth\ rate = \mu_A \left(\frac{S_{NH}}{K_{NH} + S_{NH}}\right)\left(\frac{S_O}{K_{O,A} + S_O}\right) X_{BA} \quad (4)$$

Here, μ_A is the maximum specific growth rate for autotrophic biomass, S_{NH} the concentration of ammonium, S_O the concentration of dissolved oxygen, X_{BA} the concentration of autotrophic biomass, K_{NH} the half saturation index of ammonium and $K_{O,A}$ is the half saturation index of dissolved oxygen for autotrophic biomass.

TIS modelling

A simple and standalone TIS model for the bioreactor (only outer ring) of the WRRF was developed in order to draw a comparison between TIS and CFD modelling. The reactor was divided into six tanks based on reactor's configuration and is shown in Appendix 2a. Each of the tanks was named according to its configuration and function. In the Appendix 2a, T_{in} is the section having the inlet, T_{an1} is thanoxic section before winter package, T_W is the winter package section, T_{an2} is the anoxic section between summer and winter packages, T_S is the summer package and T_{out} is the section having the outlet and recycle pumps. Steady-state simulations were then performed in the modelling and simulation platform WEST (MikebyDHI) with the default K-values and same influent composition and flowrates as of the CFD simulations. The respective plant layout in WEST is shown in Appendix 2b. (Appendix 2 is available with the online version of this paper.)

RESULTS AND DISCUSSION

The results from CFD hydrodynamic and CFD-biokinetic model are discussed separately in the following sections. Moreover, the comparison between TIS and CFD results is also presented and described.

CFD hydrodynamic model results

The absolute velocity magnitudes derived from the ADCP-measured tangential and axial fluid velocity components along with the corresponding CFD predictions at the B2 locations are shown in Figure 2(a). As can be seen, velocity profiles at locations B and C are overpredicted, although the trends with respect to depth are evident. The underlying causes for this overprediction could be several. It is particularly important to note that the velocity data were collected under dynamic hydraulic conditions, whereas the model was run at steady-state conditions using an average inflow rate. Whether this is the only cause for model-experiment divergence would require further investigation. Preliminary

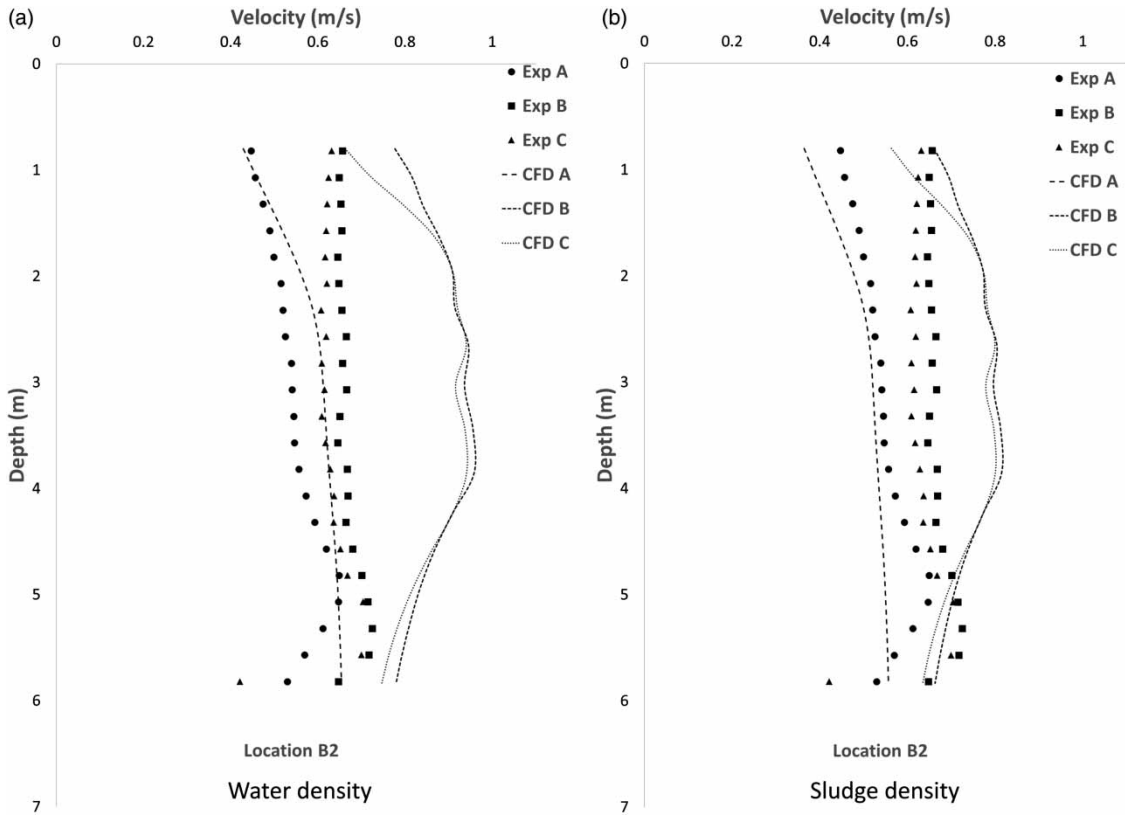

Figure 2 | Comparison between the predicted and measured velocities at the location B2 (A: near the inner wall, B: in the middle and C: near the outer wall) (average measurement error is ±0.0315 m/s) for (a) water density and (b) sludge density.

investigation showed that the overprediction was reduced by 10–15% when using the bulk density function (Figure 2(b)), instead of the standard water density, indicating the importance of using an appropriate density.

In Figure 3(a) and 3(b) liquid velocities and air volume fractions are shown for horizontal cross sections of the reactor (3.45 m of depth), respectively. In these figures, flow variations and non-ideal mixing in the reactor can be observed even in areas close to propellers and the aeration system (summer aeration package). The velocity variations in the aerated zone occur mainly due to aeration but, overall, ring shape of the reactor also tend to create a velocity gradient between the outer and inner walls throughout the reactor length. Therefore, it causes the bulk flow to move at different speeds across the width of the reactor. In Figure 3(b), it can be seen that gas holdup varies not only in direction of bulk flow but also across the width (lateral to the bulk flow) of the reactor. Moreover, the maximum gas holdup appears away from the onset of the aerated region. This is because the gas phase is not exactly moving vertically towards the water surface, but instead it is pushed along the bulk flow and that is why high gas holdup is visible even beyond the aerated region.

In order to further investigate mixing behaviour in the reactor, velocity vector plots in a vertical cross section of the reactor (in the aerated region) are shown for two different aeration rates (Figure 3(c) and 3(d)) (it should be noted that all the vertical cross section plots are taken from the same location indicated in Figure 1). The L-G case (Figure 3(c)) clearly shows macromixing patterns with one major (in the middle) and one minor (near the inner wall) 'dead' zone in the cross section that will entail lower mass transfer rates. As can be seen, in the L-3G case (Figure 3(d)), the minor dead zone disappears due to increased aeration rate. The implication of the results shown is that non-ideal mixing is ubiquitous throughout the reactor, including in the aerated region, where oxygen has to be transferred efficiently to liquid phase. These regions are averaged out when using simpler models (such as the TIS modelling); consequently, these models do not completely reflect heterogeneity of the reactor in terms of mixing and aeration. These findings are similar to observations made in previous studies (Gresch *et al*. 2011a, 2011b). Given this, it is now important to investigate what the implications are of this non-ideal mixing on local process rates and, hence, local component

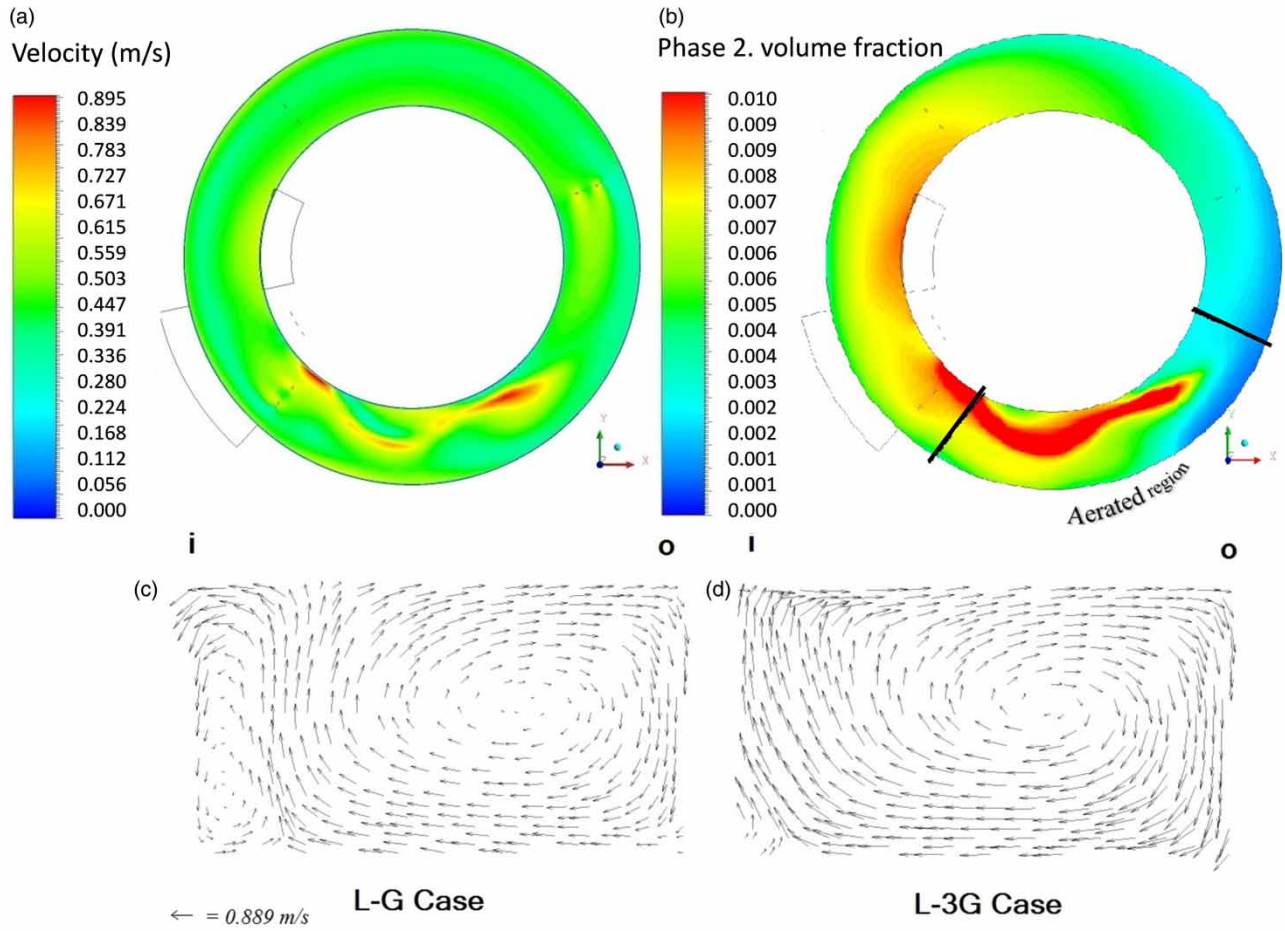

Figure 3 | (a) Velocity and (b) gas hold up (volume fraction) contour plots at 3.45 m depth in the reactor for L-G case. Velocity vector plots at the vertical cross section in the aerated region of the reactor for (c) L-G and (d) L-3G cases (plot location indicated in Figure 1).

concentrations and what consequences this has with regard to current modelling approaches to account for mixing and the need for model calibration.

CFD-biokinetic model results

Results of the local concentrations of dissolved oxygen and ammonium from CFD-ASM model are shown in Figure 4(a) and 4(b) for the horizontal and vertical cross sections (identical section as in Figure 3(a) and 3(b)). The dissolved oxygen and ammonium concentrations vary between 0.2 and 1.96 mg/L and 0.4 and 2.2 mg/L, respectively (Figure 4(a) and 4(b)). These results clearly show non-uniformity in both dissolved oxygen and ammonium concentrations throughout the biological reactor. This non-uniformity takes place also in the part of the reactor corresponding to the aeration system, where uniform mixing and substrate concentrations are typically assumed. It must be noted that the concentration variations are not only in the direction of flow but also in the directions lateral to the bulk flow (i.e. along the width of the reactor). The concentration variations along the length are obvious due to aerobic and anoxic conditions. However, the variations along the width are usually not expected and hence are ignored in conventional TIS modelling methods.

The variations across the width eventually lead to differences in concentrations near walls and in bulk flow. The outlet of the reactor is located at the wall and this heterogeneity would ultimately cause difference in ammonium and dissolved oxygen concentrations at the reactor outlet and in bulk flow. In terms of dissolved oxygen, a sensor used as input for a DO controller can lead to significantly different controller behaviour depending on its location (exactly at the outlet or in the bulk flow). The importance of sensor location has already been demonstrated by Rehman *et al.* (2015). However, simple TIS approach can only take

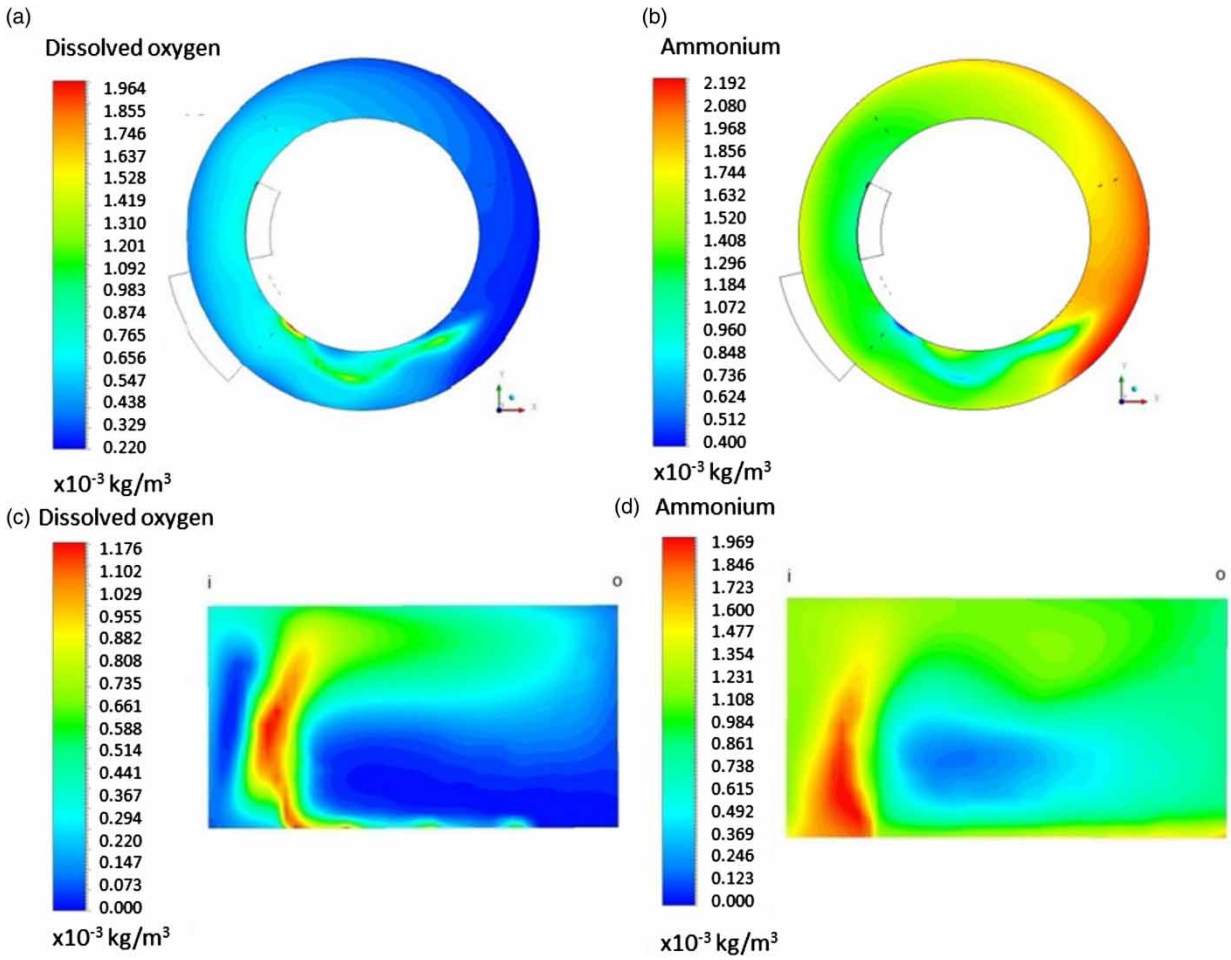

Figure 4 | (a) Dissolved oxygen and (b) ammonium concentrations at 3.45 m depth in the bioreactor. (c) The dissolved oxygen and (d) ammonium concentrations at a vertical cross section in the aerated region (plot location indicated in Figure 1) for the L-G case.

into account the variations along the flow by using more number of tanks and assumes complete mixing within each tank. The TIS models are unable to distinguish between different lateral locations of the sensor, therefore, could lead to misleading conclusions and, hence, decisions based on those.

Figure 4(c) and 4(d) show the impact of the flow patterns in a vertical cross section of the aerated region shown in Figure 3(c) and 3(d) on the local concentrations of dissolved oxygen and ammonium for the base case (L-G). These regions are considered to be well-mixed, whereas Figure 4(c) and 4(d) show a clear heterogeneity in dissolved oxygen and ammonium concentrations. The variations in dissolved oxygen concentration originate from the fact that aeration is causing a flow pattern, which creates significant recirculation. The latter creates a region within its core (dead zone) that becomes isolated from the bulk flow and thus leads to less mass transfer (from the gas to liquid phase). Therefore, the dissolved oxygen concentration is not uniform and consequently results in local variation in ammonium concentration since it is subject to an aerobic process. Similarly, these variations also affect other process variables, as well, such as nitrate and organic carbon concentrations (Appendix 3, available with the online version of this paper).

Equation (4) shows that the autotrophic growth rate depends on dissolved oxygen and ammonia concentrations, therefore, the local concentrations impact process rate locally. Appendix 4 (available online) shows the impact of concentrations shown in Figure 4(c) and 4(d) on local autotrophic growth rate in a vertical slice of the reactor in the aerated zone. As can be seen, there are major areas with significantly reduced dissolved oxygen concentrations (Figure 4(c)) leading to anoxic conditions and, hence, limiting aerobic growth of autotrophic biomass. Therefore, it is

evident that local mixing is limiting the process rate locally. However, as these details are ignored in a TIS model, reduced/enhanced process rates need to be achieved by altering half saturation indices.

Figure 5 shows averaged substrate concentrations. These averages provide the information about the performance of different sections of the reactor. Here, ammonium and dissolved oxygen concentrations have been averaged for every section of the reactor and also corresponding complete range bars (minimum and maximum values) are shown. Before evaluating these plots, the physical significance of these sections must be understood. Sections T1 and T2 are the first two sections sharing the inlet and T3 to T7 are the sections downstream from the inlet. Sections T8 to T11 are the aerated sections and T12 is the section having the outlet and recycle streams. As expected, the average dissolved oxygen concentration decreases from 0.65 mg/L in section T1 to 0.1 mg/L in section T8 (start of aerated region). Thereafter, due to aeration, the concentration again increases to 0.76 mg/L up until section T12. However, the trend in ammonium concentrations is quite different. The only source of ammonium is at the inlet (i.e. ammonium load coming into the system) and, as a result, there is an increase in its concentration from 1.3 mg/L in section T1 to 2.0 mg/L in section T2. Thereafter, the average ammonium concentration decreases almost linearly to 0.9 mg/L up until section T12. The range bars in the plots provide an indication about the magnitude of the variation in a section. The larger range bars indicate higher variations and vice versa. Figure 7 shows that these range bars differ in size moving from one section to the next. For example, the range bar of dissolved oxygen concentration in section T10 is the largest (0.1 to 1.4 mg/L) and smallest for section T7 (0 to 0.5 mg/L). Hence, the heterogeneity in dissolved oxygen concentrations in section T7 is substantially lower than in section T10. It can be concluded that different sections of the reactor have different levels of heterogeneity, which is currently not reflected in the modelling of such systems since TIS models consider complete mixing.

Scenario analysis

Figure 6(a) and 6(b) show the impact of different liquid and gas flows on the dissolved oxygen and ammonium concentrations in a vertical cross section of the aerated region, respectively. As can be seen, doubling liquid flows while keeping a constant air flow of 2,000 Nm^3/h does not cause improved mixing conditions. Significant changes are visible in terms of ammonium elimination originating from the limited availability of the air at double influent rates. Triplicating gas flows brings about significant increases in the dissolved oxygen concentrations (with consequent decreases in ammonium concentrations). Additionally, at this high gas flow rate, the interaction in terms of mixing between the air and liquid flows becomes evident. At higher liquid flow rates, an increased mixing non-uniformity prevails which would not be easy to predict without the application of CFD. These results are important to understand what will happen at the process level with dynamic influent flows, and the impact of varying gas flow rates in response to these dynamics. This information would be

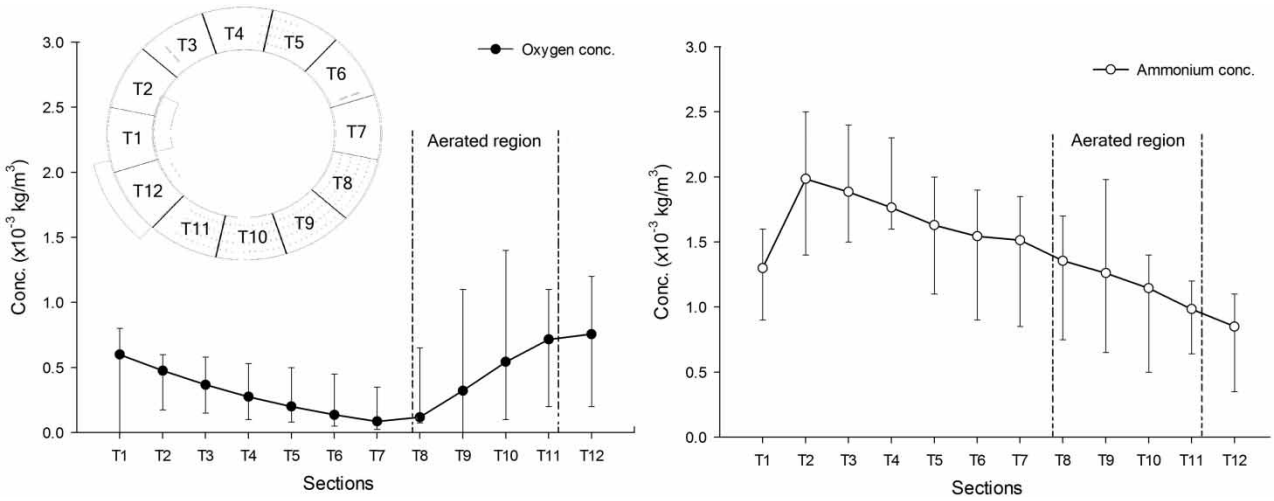

Figure 5 | Averaged ammonium and dissolved oxygen concentrations in the different sections of the reactor.

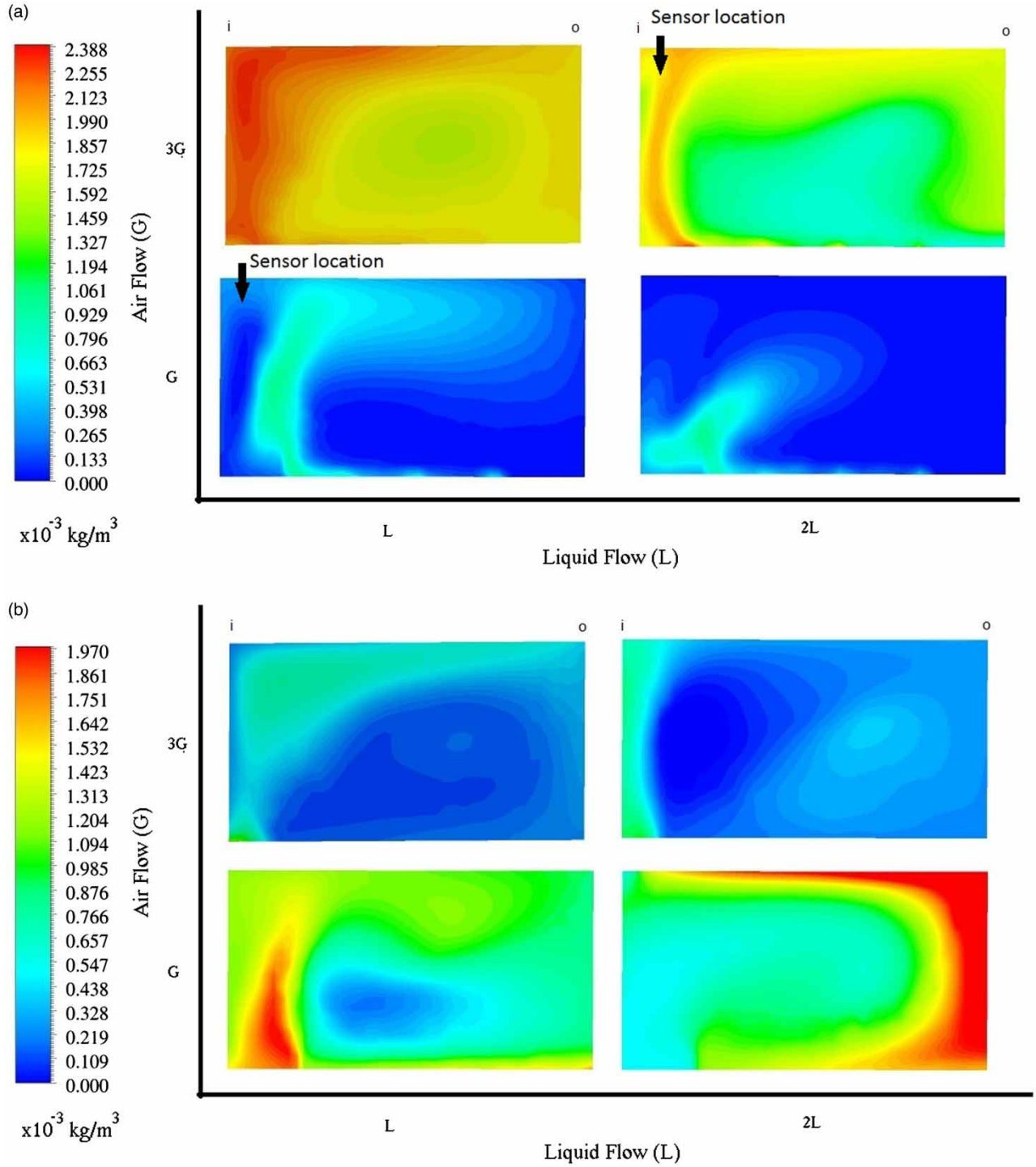

Figure 6 | Dissolved oxygen (a) and ammonium (b) concentrations in the cross section (plot location indicated in Figure 1) of the aerated region at different air and liquid flow rates.

difficult to attain without the use of an integrated hydrodynamic-biokinetic model like the one developed in the present study. The dynamics of mixing with varying liquid and air-flow rates is currently completely ignored in conventional TIS modelling.

Concentration distribution plots

In order to quantify and clearly present the heterogeneity of species, the concept of CDPs was developed. These are volume-based frequency distributions for a species. The

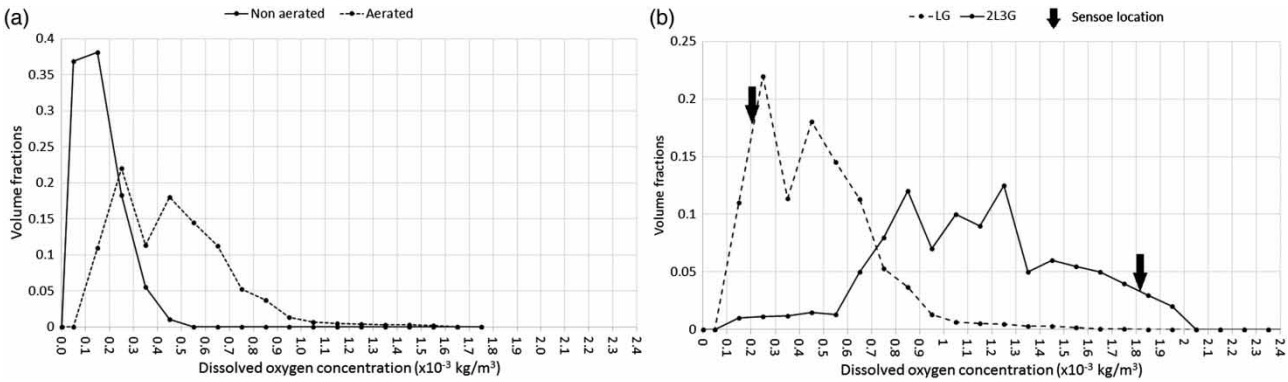

Figure 7 | Dissolved oxygen concentration distributions in different sections of the bioreactor for (a) the L-G case and (b) comparison of dissolved oxygen concentration distributions in the aerated section for different scenarios.

CDP for dissolved oxygen concentration is shown in Figure 7. Appendix 3 illustrates how the CDP is calculated from the CFD model. The CFD-biokinetic model provides local concentrations for each cell of the grid (mesh). In a certain section of the reactor with volume 'V1', for each cell 'i', the local concentrations 'Ci' and the corresponding size 'Vi' of the cell is calculated (available from the CFD-biokinetic model). Therefore, the total volume of the cells having concentration 'Ci' would be $\sum$Vi and corresponding volumetric fraction would be $\Sigma Vi/V1$. Similarly, such volumetric fractions can be calculated based on concentration ranges such as 'Ci to Ci + ΔC' and 'Ci + ΔC to Ci + 2ΔC' instead of absolute concentrations. Finally, with the knowledge of minimum and maximum concentrations and by choosing a small step change (ΔC), a CDP can be plotted for each species in a user-selected volume 'V1'. Hence, for each volumetric region selected by the user, a CDP can be constructed and this, for every species, computed by an integrated CFD-ASM model.

The CDPs for the DO concentrations in two different sections of the reactor and under different conditions are shown in Figure 7. A step change (ΔC) of 0.1 mg/L is used for all these plots. Figure 7(a) shows the CDP for DO in the aerated and non-aerated sections of the reactor. It should be noted that the curves are merely extrapolated by joining the points which correspond to mid-points of each step change. For example, the first point in Figure 7(a) (for non-aerated CDP) represent the step change 0–0.1 mg/L, thus it is plotted at 0.05 mg/L and its y-axis value reads 0.37 (volume fraction). It can now be stated that 37% of the non-aerated region has a concentration between 0 and 0.1 mg/L. Moreover, Figure 7(a) shows that, in the non-aerated section, the DO concentration ranges between 0 and 0.6 mg/L. However, the aerated section has a dissolved oxygen concentration range between 0 and 1.4 mg/L and does not exceed 1.4 mg/L. The CDPs clearly show more heterogeneity in the aerated section as compared to the non-aerated one, which could be expected but has now been quantified.

Figure 7(b) shows CDPs for dissolved oxygen in the aerated section but for the two different scenarios (i.e. L-G and 2 L-3G). The variation in dissolved oxygen distributions due to changes in operational conditions is evident. In the case of the 2 L-3G scenario, the CDP is extensively spread and, thus, the use of a completely mixed assumption will not be a good estimate of the entire tank behaviour under such conditions. Depending on the final objective of the modelling study this loss of detail could be acceptable or, on the contrary, could bring about incomplete and/or incorrect process conclusions or lead to significant calibration efforts.

In order to investigate the actual impact of heterogeneous concentrations on the process rates, Appendix 4 shows distributions for the process rate (autotrophic growth rate). A step change of 0.005 ($\times 10^{-4}$ kg/m^3·s) is used for these distributions. It can be seen that the distribution of autotrophic growth rate is more non-uniform for the aerated section as compared to the non-aerated section. For the aerated section, the growth rate CDP spreads between 0.018 and 0.07 ($\times 10^{-4}$ kg/m^3·s), whereas, in the non-aerated section it is between 0 and 0.02 ($\times 10^{-4}$ kg/m^3·s). Similar observations can be made for the different scenarios in Appendix 6b (available online). The CDPs in the case of 2 L-3G show that the growth rate distribution is more non-uniform as compared to the L-G case. These findings are similar to the findings in Figure 7 with respect to non-uniformity among the different sections of the reactor as well as among the different operational conditions.

Comparison between the TIS and CFD modelling

In order to compare the CFD results with conventional TIS modelling results, the CFD concentrations were averaged over different sections of the reactor as shown in Appendix 2a. The comparison between the TIS and CFD was performed for two cases i.e. L-G and 2 L-3G. The resulting dissolved oxygen and ammonium concentrations for both modelling approaches under two different operational conditions is shown in Figure 8. It must be noted that the TIS model assumed complete mixing in each of these sections. In contrast, average values from the CFD model are based on local concentrations taking into account mixing limitations and hence can be considered as a true representation of an average behaviour of the tanks. Notice that these average values are similar to the values plotted in Figure 5 but with different number of tanks. Moreover, maximum and minimum bars are not shown here to not overload the figures. For clarity, the results for both cases are discussed separately.

In the L-G case, it can be seen that TIS model predicted lower DO concentrations compared to CFD model. This is due to the fact that the TIS assumed complete mixing in each tank and thus overestimated oxygen consumption resulting in lower DO concentrations. However, the CFD model took into account mixing limitations and hence resulted in higher DO concentrations. The trend in DO concentrations is, however, similar in both models until the aerated tank (T_S). Further downstream in the outlet region (T_{out}), the DO concentrations decrease to 0.25 mg/L in the case of the TIS model but increase to 0.75 mg/L in the case of the CFD model. This can be understood by considering the underlying flow patterns and mixing limitations inside the reactor shown in Figure 4. Figure 3(b) shows that the gas holdup is pushed in the direction of bulk flow and hence a high DO concentration is observed in the outlet region (Figure 4(a)). This results in a higher average CFD DO concentration in Figure 8 in the T_{out}. However, the TIS model is unable to take into account the impact of local hydrodynamics and thus predicts low DO concentration. Similarly, ammonium concentrations are also lower for the TIS model due to the assumption of complete mixing. It is also important to note that the TIS model predicts 0.52 mg/L ammonium in the T_{out} which is eventually considered effluent concentration, whereas the CFD model predicts 0.9 mg/L ammonium concentration in T_{out} and 0.82 mg/L in effluent (i.e. average over the outlet of the bioreactor).

In the 2 L-3G case, the difference between the TIS and the CFD average values is even larger than in the L-G case. This is because the TIS model ignored the impact of operational conditions on the hydrodynamics but the CDP distributions (Figure 7(b)) for the 2 L-3G case displayed a wider distribution of the DO concentrations compared to the L-G case and, hence, a larger degree of heterogeneity. Therefore, it verifies the obvious that larger heterogeneity leads to larger deviation from the complete mixing assumption. Moreover, again the TIS model predicted lower DO concentrations compared to the CFD model except for the aerated region. In the aerated region (T_S), it could be due to the impact of bulk flow, as well as due to mixing limitations caused by the dead zones. It can be noticed that, for the CFD model, the DO concentration in the outlet and inlet regions is quite high compared to the other regions due to this.

These results show that the heterogeneities observed in the CFD-biokinetic model are hugely averaged out in the TIS model. For example, for L-G case, the TIS model predicted 0.37 mg/L DO concentration in the aerated region; however, Figure 7 shows that the DO concentration in the

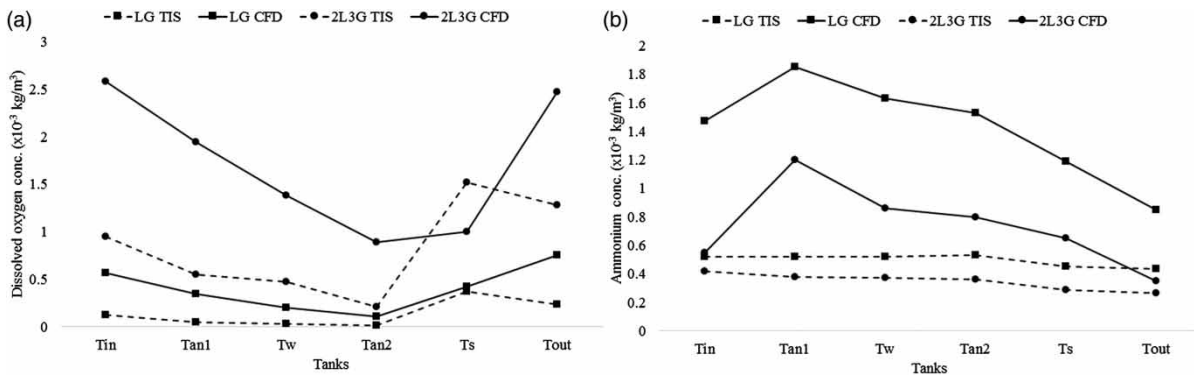

Figure 8 | Comparison between the TIS and CFD modelling for dissolved oxygen (a) and ammonium concentrations (b).

aerated region ranges between 0 and 1.4 mg/L. Similarly, for the 2 L-3G case, the TIS model predicted 1.5 mg/L in the aerated region but Figure 7(b) shows that DO concentration range between 0 and 2.1 mg/L. Hence, the TIS model values are not a good representative of the average tank behaviour as seen in Figure 8 and, therefore, mostly need calibration of the half saturation indices to fit the measurements.

In addition to the comparison between the concentrations, the autotrophic growth rates are calculated for both models under different operational conditions (L-G and 2 L-3G). The results are shown in Appendix 7 (available online). It should be noted that the process rates for the CFD model are volume-weighted average process rates calculated from the local concentrations. The process rates predicted by the TIS model are less than the CFD based process rates. Moreover, Appendix 4 shows that the growth rate is not uniform and has a distribution similar to the concentration distributions. For example, in the aerated tank (TS), the TIS predicted 0.013 ($\times 10^{-4}$ kg/m^3·s) to be the process rate, whereas Appendix 6a shows that it varies between 0.018 and 0.07 ($\times 10^{-4}$ kg/m^3·s). The difference between the TIS and the volume-averaged process rates can help in providing an insight about how much calibration will be needed for the TIS model. It can also provide a basis to devise a protocol for calibration procedures taking spatial variations and flow dynamics into consideration.

Sensor placement/reading and calibration

The comparison between the TIS and CFD displayed the imminent need of calibration for the TIS model to correct for the errors induced due to the assumption of complete mixing.

In the TIS modelling techniques, the $K_{O,A}$ (half saturation index of oxygen for aerobic growth of autotrophs) values are calibrated based on a measured dataset, collected at a specific (easily accessible) location in a reactor. The model should be able to take the sensor location into account for a robust calibration effort. The TIS model can take into account the location of sensor to a certain extent but is unable to distinguish between lateral locations of the sensors. However, Figure 6 shows that the measured dataset would be highly dependent on the sensor location (due to spatial variations across the cross section). Therefore, resulting calibrated $K_{O,A}$ values would potentially be different for different physical sensor locations in the bioreactor.

Moreover, the hydrodynamic results showed a change in flow patterns with the change in operational conditions (Figure 3(c) and 3(d)) and their impact on the concentrations (Figure 6). This can potentially impact the sensor measurements and hence the calibration. One can investigate this by assuming a fixed sensor location to be close to the inner wall (Figure 6) in the aerated section. For the L-G case, the measured DO concentration would be 0.22 mg/L (Figure 6), whereas the TIS model predicts 0.4 mg/L for the aerated tank (T_S) (Figure 8). Therefore, for the L-G case, measured DO is lower than DO predicted by the TIS model. However, for the same sensor location in the 2 L-3G case, measured DO (1.82 mg/L) is higher than the DO (1.5 mg/L) predicted by the TIS model (Figure 8). Therefore, in order to calibrate TIS model, for the L-G case, the $K_{O,A}$ value will have to be reduced, whereas for the 2 L-3G case, it needs to be increased to fit dynamically measured data (meaning that no single calibrated K-value can be found). Similarly, calibration of other half saturation indices will also depend on local mixing conditions.

In addition, Figure 7(b) provides the information about the sensor measurement/placement with respect to the CDPs under the different operational conditions. As the CDPs were drawn for a range of concentrations (step change), therefore, it is important to indicate the step change where the measured value belongs. The sensor measurement for the L-G case is 0.22 mg/L, thus it corresponds to the 0.2–0.3 range. Hence, it can be said that the measured value represents at maximum 23% of the aerated region. Similarly, the sensor measurement for the 2 L-3G case at maximum represents only 4% of the aerated region. Therefore, relatively, the sensor measurements for the L-G case would be more reliable (in terms of representativeness of tank behaviour) as compared to the 2 L-3G case. This information can certainly be useful while deciding the sensor location, accounting for this in control actions and for potential calibration efforts. The impact of the sensor location and the need of recalibration while extrapolating model results to different operational conditions, such as from dry to wet weather conditions, are often ignored. Here, we clearly illustrate what this leads to and show why dynamic calibration with a fixed mixing model does not work, i.e. never results in a single parameter set describing the system under both dry and wet weather conditions.

One major reason behind the calibration of K-values is the inability of TIS based ASM models to account for local hydrodynamics. Thus, it is quite probable that these

limitations are lumped into the K-values and, hence, the default K-values being used are overestimated. However, as it is shown, the CFD takes local mixing limitations into account, thus true K-values would likely be lower than the currently employed default values in the integrated model. Therefore, Appendix 8 (available online) shows the impact of reducing the half-saturation index of dissolved oxygen ($K_{O,A}$) for autotrophic organisms by 15% on both local dissolved oxygen concentration and autotrophic growth rate. This can be regarded as a reduction in 'resistance' that a molecule senses when moving from the bulk to the cell internal (Arnaldos *et al.* 2015) as the advective portion is inherently accounted for by the CFD model. The reduction in $K_{O,A}$ value increases the growth rate (Appendix 8b) and thus in turn increases the dissolved oxygen uptake resulting in lower dissolved oxygen concentrations. These results are a mere illustration of how the reduced $K_{O,A}$ values will locally impact the process rate and concentrations. Proper determination will need detailed data collection at different locations in the reactor.

TIS models after calibration are usually used to evaluate control strategies under different process conditions or with different design configurations. However, it is shown that the a calibrated TIS model would not hold true for another set of operational conditions and would thus need recalibration. Moreover, it is most likely that a different aerator or propeller design would result in different mixing conditions which TIS models are not able to account for and hence again recalibration will be needed. Here one can argue about having a dynamic K-value TIS model i.e. different K-values under different conditions. However, this would lead to major uncertainties while troubleshooting or optimizing a plant operation. One would not be able to distinguish whether problems in the plant operation arise due to biological limitations or mixing limitations and hence will be vulnerable towards taking wrong decisions.

General discussion

The impact of these findings on the way WRRFs are currently modelled could be significant depending on the final objective of the modelling study.

It is shown that operational conditions influence the process performance in terms of ammonium removal and dissolved oxygen concentrations. Local concentration gradients exist in the reactor and current modelling methods (i.e. TIS modelling) are unable to account for them (as seen in Figure 8). This inadequacy of TIS models can lead to erroneous outputs and, hence, wrong decisions. However, detailed modelling such CFD-ASM modelling can be useful for detailed process design, evaluation and optimization. For instance, aerator design and placement for optimal process performance would benefit from the CFD-ASM model developed in this study; conventional process engineering does not address the heterogeneities in the dissolved oxygen and contaminant concentrations caused by different aerator configurations and operational regimes. Similarly, knowledge of local substrate conditions is required in order to make appropriate decisions in terms of sensor location for both process monitoring and control. Aerated zones are commonly perceived as homogeneously mixed; sensor location is, thus, normally decided upon driven by maintenance and operation convenience. Even though this should still be considered when deciding sensor location, it has been clearly shown that different locations along the width and depth of the reactor will bring about significantly different concentration measurements. Therefore, the information shown will be necessary to carry out decisions regarding appropriate sensor placement and its impact on controller performance by accounting for this in the control algorithm (e.g. use of a different setpoint). Additionally, the results presented have far-reaching consequences in terms of process evaluation. For instance, phosphorus removal has been widely documented in systems with no anaerobic sections, such as aerobic membrane bioreactors (Rosenberger *et al.* 2002; Verrecht *et al.* 2010; Barnard *et al.* 2012). The modelling results presented provide evidence that this could be due to the existence of anaerobic zones in the reactor, even in places supposedly aerated and well mixed. In the specific case of MBR, sludge rheology becomes more important which can be accounted for in a CFD setting. Another example where heterogeneous mixing could be of importance is in simultaneous nitrification-denitrification (SND) processes (and the rest of the nitrogen conversion processes taking place at low dissolved oxygen concentrations and leading to N_2O production). Even though SND has been largely attributed to diffusion limitation in flocs (Münch *et al.* 1996), from the results presented here, it is evident that non-uniform mixing will definitely also play a significant (and maybe even a leading) role.

In general, the previous discussion underlines the fact that an integrated ASM-CFD model approach provides extremely useful and detailed information about system behaviour, which can be adopted in process understanding, improved design, optimisation and process evaluation. It is therefore recommended to use this information to revise

certain conclusions taken with models that ignore mixing heterogeneity or start using models that better describe the reactor's mixing behaviour by means of compartmental models which we will address in future work.

CONCLUSIONS

In the present study, an integrated hydrodynamic-biokinetic model has been developed to describe the aerated compartment of a full-scale wastewater treatment plant. The model incorporates the detailed oxygen mass transfer using constant bubble size and local gas holdup. The model also takes into account local density variations as a function of local suspended solids concentrations. It was found that density has a significant impact (10–15% improvement in velocity predictions) on the hydrodynamics of the bioreactor. Furthermore:

- Regions of bad mixing resulting in non-uniform substrate (e.g. ammonium) and electron acceptor (e.g. dissolved oxygen) concentrations were shown to exist in areas commonly assumed to be well mixed.
- The effects of changing influent and air flows on the substrate and electron acceptor distributions have been investigated. It was observed that a single TIS mixing model would not suffice for dynamic operational conditions and there would be a potential need of recalibration of half-saturation values for TIS-based biokinetic models when moving from dry to wet weather conditions.
- The impact of sensor location on the corresponding measurements was evaluated and quantified; it was observed that the reliability of sensor measurement changed with the variation in the operational conditions.
- The presented findings can have far-reaching consequences in the terms of optimal sensor location, control system design and process evaluation.

ACKNOWLEDGEMENTS

The authors would like to thank Dr Dave Kinnear for providing the ADCP device for velocity measurements. The research leading to these results has received funding from the People Program (Marie Curie Actions) of the European Union's Seventh Framework Programme FP7/2007–2013, under REA agreement 289193 – Project SANITAS. This publication reflects only the authors' views and the European Union is not liable for any use that may be made of the information contained therein.

REFERENCES

Alex, J., Tschepetzki, R., Jumar, U., Obenaus, F. & Rosenwinkel, K. 1999 Analysis and design of suitable model structures for activated sludge tanks with circulating flow. *Water Science and Technology* **39** (4), 55–60.

Alex, J., Kolisch, G. & Krause, K. 2002 Model structure identification for wastewater treatment simulation based on computational fluid dynamics. *Water Science and Technology* **45** (4–5), 325–334.

Amerlinck, Y. 2015 Model Refinements in View of Wastewater Treatment Plant Optimization: Improving the Balance in Sub-Model Detail. Doctoral dissertation. Ghent University, Belgium.

ANSYS Inc. 2011 ANSYS FLUENT Theory Guide. Canonsburg, PA, USA.

Arnaldos, M., Amerlinck, Y., Rehman, U., Maere, T., Van Hoey, S., Naessens, W. & Nopens, I. 2015 From the affinity constant to the half-saturation index: understanding conventional modeling concepts in novel wastewater treatment processes. *Water Research* **70**, 458–470.

Atif, A., Benmansour, S. & Bois, G. 2010 Numerical investigation of velocity flow field inside an impeller air model of a centrifugal pump with vaned diffuser interactions and comparison with PIV measurements. *International Journal of Rotating Machinery* **4**, 1–12.

Barnard, J., Houweling, D., Analla, H. & Steichen, M. 2012 Saving phosphorus removal at the Henderson NV plant. *Water Science and Technology* **65** (7), 1318–1322.

De Clercq, B. 2003 Computational fluid dynamics of settling tanks: Development of experiments and rheological, settling and scraper submodels., BIOMATH, Ghent University, Belgium.

Fayolle, Y., Cockx, A., Gillot, S., Roustan, M. & Héduit, A. 2007 Oxygen transfer prediction in aeration tanks using CFD. *Chemical Engineering Science* **62** (24), 7163–7171.

Fenu, A., Guglielmi, G., Jimenez, J., Spèrandio, M., Saroj, D., Lesjean, B., Brepols, C., Thoeye, C. & Nopens, I. 2010 Activated sludge model (ASM) based modelling of membrane bioreactor (MBR) processes: a critical review with special regard to MBR specificities. *Water Research* **44** (15), 4272–4294.

Glover, G. C., Printemps, C., Essemiani, K. & Meinhold, J. 2006 Modelling of wastewater treatment plants – how far shall we go with sophisticated modelling tools? *Water Science and Technology* **53** (3), 79–89.

Gresch, M., Armbruster, M., Braun, D. & Gujer, W. 2011a Effects of aeration patterns on the flow field in wastewater aeration tanks. *Water Research* **45** (2), 810–818.

Gresch, M., Braun, D. & Gujer, W. 2011b Using reactive tracers to detect flow field anomalies in water treatment reactors. *Water Research* **45** (5), 1984–1994.

Hauduc, H., Rieger, L., Oehmen, A., van Loosdrecht, M. C. M., Comeau, Y., Héduit, A., Vanrolleghem, P. A. & Gillot, S. 2013 Critical review of activated sludge modeling: state of process

knowledge, modeling concepts, and limitations. *Biotechnology and Bioengineering* **110** (1), 24–46.

Henze, M., Grady, C. P. L. J., Marais, G. & Matsuo, T. 1987 *Activated Sludge Model No. 1*, Scientific and Technical Report No. 1, London, UK.

Henze, M., Gujer, W. & Mino, T. 2000 *Activated Sludge Models ASM1, ASM2, ASM2D and ASM3*, IWA Publishing, London, UK.

Higbie, R. 1935 The rate of absorption of a pure gas into a still liquid during short periods of exposure. *Transactions of the American Institute of Chemical Engineers* **31**, 365–389.

Ishii, M. & Hibiki, T. 2011 *Thermo-Fluid Dynamics of Two-Phase Flow*, Springer New York, NY, USA.

Laurent, J., Samstag, R. W., Ducoste, J. M., Griborio, A., Nopens, I., Batstone, D. J., Wicks, J. D., Saunders, S. & Potier, O. 2014 A protocol for the use of computational fluid dynamics as a supportive tool for wastewater treatment plant modelling. *Water Science and Technology* **70** (10), 1575–1584.

Le Moullec, Y., Potier, O., Gentric, C. & Leclerc, J. P. 2011 Activated sludge pilot plant: comparison between experimental and predicted concentration profiles using three different modelling approaches. *Water Research* **45** (10), 3085–3097.

Lyn, D., Stamou, A. & Rodi, W. 1992 Density currents and shear-induced flocculation in sedimentation tanks. *Journal of Hydraulic Engineering* **118** (6), 849–867.

Manninen, M., Taivassalo, V. & Kallio, S. 1996 On the mixture model for multiphase flow. VTT Publications 288, Technical Research Centre of Finland, Espoo, Finland.

Monod, J. 1942 *Recherches sur la croissance des cultures bactériennes*, Hermann & Cie, Paris, France.

Münch, E. V., Lant, P. & Keller, J. 1996 Simultaneous nitrification and denitrification in bench-scale sequencing batch reactors. *Water Research* **30** (2), 277–284.

Rehman, U., Vesvikar, M., Maere, T., Guo, L., Vanrolleghem, P. A. & Nopens, I. 2015 Effect of sensor location on controller performance in a wastewater treatment plant. *Water Science and Technology* **71** (5), 700–708.

Rosenberger, S., Krüger, U., Witzig, R., Manz, W., Szewzyk, U. & Kraume, M. 2002 Performance of a bioreactor with submerged membranes for aerobic treatment of municipal waste water. *Water Research* **36** (2), 413–420.

Samstag, R. W. & Wicklein, E. A. 2014 A protocol for optimization of activated sludge mixing. In: *Proceedings of the Water Environment Federation 2014* (13), New Orleans, LA, USA, pp. 3614–3640.

Samstag, R. W., Wicklein, E. A., Reardon, R. D., Leetch, R. J., Parks, R. M. & Groff, C. D. 2012 Field and CFD analysis of jet aeration and mixing. In: *Proceedings of the Water Environment Federation, 2012* (12), New Orleans, LA, USA, pp. 4113–4139.

Stamou, A., Latsa, M. & Assimacopoulos, D. 2000 Design of two-storey final settling tanks using mathematical models. *Journal of Hydroinformatics* **2** (4), 235–245.

Talvy, S., Cockx, A. & Liné, A. 2007 Modeling hydrodynamics of gas–liquid airlift reactor. *AIChE Journal* **53** (2), 335–353.

Verrecht, B., Maere, T., Benedetti, L., Nopens, I. & Judd, S. 2010 Model-based energy optimisation of a small-scale decentralised membrane bioreactor for urban reuse. *Water Research* **44** (14), 4047–4056.

Versteeg, H. K. & Malalasekera, W. 2007 *An Introduction to Computational Fluid Dynamics*. Pearson Education Ltd, Harlow, UK.

Wilcox, D. C. 1998 *Turbulence Modeling for CFD*, DCW industries La Canada, CA, USA.

First received 6 February 2017; accepted in revised form 18 May 2017. Available online 1 June 2017